Threonine phosphorylation regulates the molecular assembly and signaling of EGFR in cooperation with membrane lipids

Ryo Maeda[1], Hiroko Tamagaki-Asahina[2], Takeshi Sato[2], Masataka Yanagawa[1], and Yasushi Sako[1,3,*]

[1]Cellular Informatics Laboratory, RIKEN CPR, Wako, Saitama 351-0198, Japan; [2]Kyoto Pharmaceutical University, 5, Misasagi-cho, Yamashina, Kyoto, 607-8414, Japan; [3]CREST JST, 4-1-8, Honcho, Kawaguchi, 332-0012, Japan

*To whom correspondence should be addressed. E-mail: sako@riken.jp

Abstract

The cytoplasmic domain of the receptor tyrosine kinases (RTKs) plays roles as a phosphorylation enzyme and a protein scaffold but the regulation of these two functions is not fully understood. We here analyzed assembly of the transmembrane (TM)-juxtamembrane (JM) region of EGFR, one of the best studied species of RTKs, by combining single-pair FRET imaging and a nanodisc technique. The JM domain of EGFR contains a threonine residue that is phosphorylated after ligand association. We observed that the TM-JM peptides of EGFR form anionic lipid-induced dimers and cholesterol-induced oligomers. The two forms involve distinct molecular interactions, with a bias towards oligomer formation upon threonine phosphorylation. We further analyzed the functions of whole EGFR molecules, with or without a threonine to alanine substitution in the JM domain, in living cells. The results suggested an autoregulatory mechanism in which threonine phosphorylation of the JM domain causes a switch from kinase activation dimers to scaffolding oligomers.

Introduction

Epidermal growth factor receptor (EGFR) is an RTK responsible for cell proliferation and differentiation (1, 2) and consists of five domains; an extracellular domain that interacts with extracellular ligands, a single-pass transmembrane (TM) helix, a juxtamembrane (JM) domain, a cytoplasmic kinase domain, and a C-terminal tail domain for interaction with various cytoplasmic proteins (3, 4). Ligand association changes the conformation of EGFR in its extracellular domain (5) and induces formation of an asymmetric dimer of the intracellular kinase domains (6). This dimerization subsequently results in the phosphorylation of tyrosine residues on the tail domain and the recruitment of intracellular signal proteins such as GRB2 and PLCγ containing SH2 and/or PTB domains (7). Although the atomic structures of most of the EGFR domains excluding the tail domain have been elucidated individually (5, 6, 8-10), the overall architecture of this protein has not yet been revealed, leaving several unanswered questions about the molecular mechanisms underlying its functions. The correlation between the arrangement of EGFR molecules and their function is therefore still controversial, e.g., it has long been established that the dimerization of EGFR is necessary and sufficient for kinase activation (11), whereas several studies have reported the importance of higher-order oligomerization for EGFR-mediated signal transduction (12-14).

The TM helix and the JM domain (TM-JM) of EGFR play important roles in the conformational coupling of ligand binding to its activation and oligomerization (9, 11, 15). Previous NMR studies and molecular dynamics simulations have suggested that the TM domain forms an α-helix dimer that undergoes a configuration change following the ligand association with its extracellular domains (16, 17). This information regarding conformational changes in the TM dimer is then transmitted to the JM domain which comprises a JM-A (N-terminal half) region that can form an antiparallel helix dimer, and a JM-B (C-terminal half) region which makes intramolecular contact with the kinase domain (11). Both these JM regions contribute to the stable formation of an asymmetric kinase dimer conformation, which is crucial for kinase activation. The JM-A domain is rich in Lys and Arg residues, several of which are thought to interact with anionic lipid molecules of the plasma membrane and promote antiparallel dimer formation (18-20). In addition to the phospholipid species, cholesterol is a major component of the plasma membrane, mainly distributed as lipid rafts and caveolae, and has been implicated in the regulation of membrane fluidity and receptor function. Previous studies have shown that EGFR molecules are clustered in lipid rafts (14, 21), suggesting an interaction with cholesterols. Of note in this regard, it has been reported that the depletion of cholesterols induces various effects on EGFR signaling, also this remains controversial (22-24).

Another important factor in the regulation of EGFR through the TM-JM is the phosphorylation of Thr654 at the JM-A domain. Although Thr phosphorylation is known to be involved in EGFR deactivation, the precise mechanism of this is still elusive (25).

In our present study, by combining single-pair FRET measurements and nanodisc technology, we studied how the functions of anionic lipids, cholesterols, and EGFR Thr654 phosphorylation (pT654) are orchestrated to achieve the regulation of dimerization and/or oligomerization of EGFR. We previously reported that anionic lipids cause the dimerization of JM domains, and that pT654 together with acidic lipids induces the dissociation of the EGFR dimer (19). In this current study, we report that both the TM and JM protomers of EGFR are positioned closer to each other in the presence of cholesterols than in the EGFR dimers promoted by anionic lipids. Furthermore, we found that TM-JM peptides were oligomerized in cholesterol containing membranes, which was promoted by pT654. Finally, in living cells expressing whole EGFR molecules, we observed differential functional roles of this crucial signaling factor that are dependent on the pT654 levels.

Results

Incorporation of TM-JM peptides into nanodiscs

Synthesized peptides of the TM-JM region of EGFR were prepared and labeled with a fluorophore Cy3 or Cy5 at the N-terminus (TM terminal region) or C-terminus (JM terminal region), respectively (Fig. 1a). The peptides were reconstituted into nanodisc structures with membrane scaffold proteins (MSPs) and lipid molecules (Fig. 1b, c). Mixtures of POPC (PC), POPS (PS), and cholesterol were used for reconstruction (Fig. 1d). The nanodiscs containing cholesterol showed two peaks following size exclusion gel chromatography, one of which had a smaller disc size relative to that without cholesterol (Fig. 1e). To avoid the effects of disc size, we collected and used nanodiscs involved in the first peak fraction which had a similar size without cholesterol. Synthesized TM-JM peptides with pT654 were also reconstituted into nanodiscs. The nanodisc construction was examined under a transmission electron microscope (Fig. 1f). In total, 16 types of nanodiscs were applied to subsequent single-molecule measurements.

TM-TM interaction in the EGFR dimer

Nanodiscs containing Cy3 and Cy5-labeled peptides were immobilized onto glass surfaces and illuminated with a 532-nm laser for Cy3 excitation. A portion of the fluorescent spots contained Cy5 fluorescence derived from the occurrence of FRET (Fig. 2a, b). Based on the fluorescence intensity, we selected nanodiscs containing one Cy3- and one Cy5-labeled peptide and calculated the FRET efficiency, E_{FRET} (Fig. 2c).

We first examined the interactions between the N-terminal regions of the TM domains (Fig. 3). When Thr654 was not phosphorylated and the membrane contained only PC as lipid species, E_{FRET} distributed with a peak at a relatively high (> 0.90; Table I) value (Fig. 3a), indicating close proximity of the two TM domains. There may be additional stable structures between the TM domains, as suggested by the small peaks and shoulders in the E_{FRET} distribution. The addition of anionic lipid PS caused few effects, i.e., the TM dimers were maintained as the major structure (Fig. 3b). Peptides with pT654 slightly decreased the major peak positions of the E_{FRET} distributions in the PC or PC/PS membranes (Fig. 3e, f). The smooth distribution of the pT654 peptides suggested that pThr654 had homogenized possible substructures of the TM dimers of non-phosphorylated peptides. PS had a little effect on the TM-TM interactions regardless of the Thr654 phosphorylation. The presence of cholesterol in the membrane concentrated the distributions to a high E_{FRET} (> 0.95) region (Fig. 3c, g, h), indicating that the N-terminal regions of TM-TM dimers were positioned in extremely close proximity. Although the peak position was similar in PC and PC/cholesterol membranes (Fig 3a, c;

Table I), the distribution in PC/cholesterol membrane was more accumulated to the peak position. It also should be noted that the accumulation at a high E_{FRET} region was a remarkable observation for pT654 peptides. Thus, pT654 and the presence of membrane cholesterol decreased the distance between the two N-termini of the TM domains in cooperation. PS competed with cholesterol when Thr654 was non-phosphorylated (Fig. 3d).

JM-JM interaction in the EGFR dimer

To examine the effects of lipid species and pT654 on JM-JM interaction, E_{FRET} distributions were determined under the C-terminus labeling (Fig. 4). In PC membrane, E_{FRET} was broadly distributed with a peak around 0.81 (Fig. 4a; Table I). It is plausible that the JM-A dimers are fluctuating between minor dissociation and major association states. In the PC/PS membrane, the peak fraction was increased, indicating that PS stabilized the JM-A dimer conformation (Fig. 4b). pThr654 increased the low FRET fraction in the PC/PS membrane (Fig. 4f) but showed little effect in the PC membrane (Fig. 4e). These results confirmed the results of our previous study (19). Cholesterol moved the E_{FRET} peak between non-phosphorylated peptides to higher values (0.93–0.94) regardless of whether it was a PC or PC/PS membrane (Fig. 4c, d), i.e., cholesterol forced the C-termini of the JM-A domains to position closer.

The mixed effects of cholesterol and pT654 on the JM-JM interaction were further examined. In the PC membrane (Fig. 4g), cholesterol increased the high FRET population to a comparable level to those shown for non-phosphorylated peptides. Cholesterol in the PC/PS membrane (Fig. 4h) reversed the E_{FRET} distribution seen in the PC/PS membrane without cholesterol (Fig. 4f) to that observed in the PC membrane (Fig. 4e) i.e. minor low FRET and major high FRET states in the PC/PS/cholesterol membrane. However, it should be noted that the E_{FRET} values were not as large as those found in other conditions with cholesterol (Fig. 4c, d, g), i.e., the cholesterol effect on JM-JM interaction was partially diminished by the coexistence of PS and pThr654. Overall, our data showed that cholesterol increased the proximity between the C-terminus of JM domains in PC and PC/PS membranes, and that this effect overrode that of pThr654 in the PC/PS membrane.

Higher-order oligomerization of TM-JM peptides

We speculated that the accumulation of EGFR in lipid rafts, which has been reported in previous studies, could be an effect of cholesterol in the raft membrane. We examined the assembly of TM-JM peptides in the nanodiscs, collecting images of fluorescent spots

154 containing only Cy3-labeled peptides to avoid interference from the effects of FRET
155 occurring between Cy3 and Cy5. Figure 5 displays the fluorescence intensity histograms
156 of C-terminus-labeled TM-JM peptides in nanodiscs containing or not-containing
157 cholesterol. Cholesterol shifted the histograms toward higher intensities for the pT654
158 peptides (Fig. 5b, d), suggesting a cooperative effect of cholesterol and Thr
159 phosphorylation to induce higher-order assembly of the TM-JM peptides.
160
161 **Assembly of TM regions**
162 For analysis of the interactions between more than two TM or JM domains in the
163 assembled structures at the N-terminus, images of fluorescent spots containing two Cy3-
164 labeld peptides and one Cy5-labeled peptide were collected based on their 2-color
165 fluorescence trajectories (Fig. 6a). These nanodiscs showed a variety of Cy3 donor
166 fluorescence intensities before Cy5 photobleaching indicating that the three peptides
167 interacted diversely. We constructed maximum fluorescence intensity histograms in the
168 Cy3 donor channel before and after Cy5 acceptor photobleaching for inference of the
169 interactions between three TM domains (Fig. 6b–i). In all conditions other than non-
170 phosphorylated peptides in the PC/PS membrane, Cy3 distributions after Cy5
171 photobleaching (red) peaked at the fluorescence intensity of ~100 (in arbitrary units),
172 which was smaller than that observed for the C-terminal-labeled peptides (~150; Fig. 7b–
173 i). This result must have been caused by homo-FRET (self-quenching) between two N-
174 terminal labeled Cy3 peptides. Together with the very small intensity peaks prior to Cy5
175 photobleaching (blue), these distributions suggested that TM regions of the three peptides
176 (two of them were randomly labeled with Cy3) were oligomerized in very close proximity
177 to each other in the major configuration (trimer; Fig. 6j).
178 For non-phosphorylated peptides in the PC/PS membrane however (Fig. 6c), the
179 Cy3 intensity histogram after Cy5 photobleaching (red) had a peak intensity at ~150,
180 indicating that two Cy3-labeled peptides in the major population were positioned
181 separately. In addition, the low intensity shoulder in this distribution indicated the
182 presence of proximate dimers (and trimers). Taken together, these distributions suggested
183 that N-terminal regions of three non-phosphorylated peptides have a stronger tendency to
184 arrange as one dimer and one monomer in the PC/PS membrane than any other condition.
185 A similar dimer + monomer arrangement might be contained in the distributions under
186 other conditions as a minor fraction. Consistent with this suggestion, for the non-
187 phosphorylated peptides in PC/PS membrane before Cy5 photobleaching (Fig. 6c, blue),
188 a homo-FRET fraction (~100; with a low E_{FRET} to Cy5) was evident compared to other
189 conditions. It should be noted that the ability of PS to promote the dimer + monomer

190 arrangement was diminished for pT654 peptides (Fig. 6g). Cholesterol also reduced this
191 effect of PS even for non-phosphorylated peptides (Fig. 6e). As observed in the earlier
192 analysis of the TM-JM peptide dimer (Fig. 3), the effects of PS and cholesterol were
193 competitive.
194
195 **Assembly of JM regions**
196 We constructed Cy3 fluorescence intensity histograms of two Cy3 and one Cy5 peptide
197 with C-terminal-labeling in single nanodiscs in order to analyze the interactions between
198 three JM domains (Fig. 7). The distributions of the Cy3 florescence after Cy5
199 photobleaching (red) were similar under all conditions, exhibiting a single peak at ~150,
200 which was the fluorescence intensity of the two Cy3 molecules without strong
201 interactions to induce homo-FRET. Both the trimer and dimer + monomer arrangements
202 are possible if we assume that the three molecules in the trimer and two molecules in the
203 dimer are not so close that they will induce homo FRET (Fig. 7j).
204 Prior to Cy5 photobleaching (blue), the distribution peaks were observed in the
205 region of small Cy3 intensities indicating the proximity of both Cy3 molecules with Cy5
206 to induce high E_{FRET}, as observed between two molecules in a nanodisc (Fig. 4), i.e., the
207 formation of a JM trimer. An accumulation in the low intensity peak fraction was very
208 evident for non-phosphorylated peptides in the membranes containing cholesterol (Fig.
209 7d, e). On the other hand, fractions at the intensities similar to those observed after Cy5
210 photobleaching were significant for pT654 peptides in the membrane without cholesterol
211 (Fig. 7f, g). In general, pT654 peptides exhibited higher fluorescence intensity compared
212 to non-phosphorylated peptides in the corresponding membrane lipid compositions. One
213 possible explanation is that the fraction of high Cy3 intensity before Cy5 photobleaching
214 represents a Cy3 dimer in the dimer + monomer arrangement of three peptides (Fig. 7j).
215 Another possibility is that it was caused by an increased distance between three JM
216 domains in trimers, resulting from Thr phosphorylation to reduce E_{FRET} (Fig. 7j top
217 middle). These two arrangements could potentially coexist.
218 Considering the possible arrangement for the TM and JM regions of three TM-
219 JM peptides together (Figs. 6 and 7), we conclude that cholesterol induces the closely
220 proximate oligomerization of three JM domains of non-phosphorylated peptides whereas
221 PS preferentially causes a dimer + monomer arrangement, and the Thr phosphorylation
222 disrupts the JM dimer and facilitates oligomerization of peptides with separated JM
223 domains in the presence of cholesterols (Fig. 8).
224
225 **Effect of Thr phosphorylation on the Tyr phosphorylation of EGFR**

226 Our single-molecule structural analysis suggested that pT654 is a key regulator of the
227 molecular assembly of EGFR, which may affect its functions. We examined this
228 possibility in living cells. It is known that PKC activation under EGF signaling induces
229 pT654 in EGFR. This process has been thought to be a negative feedback pathway in the
230 EGFR system. We expressed a wild type (wt) or T654A mutant EGFR in CHO-K1 cells,
231 which have no intrinsic expression of EGFR. An increase in pT654 was observed for wt
232 EGFR after EGF stimulation, and treatment of these cells with phorbol-12-myristate 13-
233 acetate (PMA), a PKC activator, caused stronger phosphorylation of Thr654 regardless
234 of EGF stimulation (Fig. 9a). Application of a saturation amount (100 ng/ml) of EGF to
235 the culture medium induced phosphorylation of Tyr1068 (pY1068) of both the wt and
236 T654A mutant EGFR proteins (Fig. 9b). pY1068 is a major association site on EGFR for
237 the adaptor protein GRB2 and its levels after EGF stimulation were significantly
238 increased by the T654A mutation compared to wt, as expected from the negative effect of
239 pT654, whereas pretreatment with PMA decreased the pY1068 level in both the wt and
240 T654A mutant EGFR (Fig. 9c). The PMA-induced decrease in pY1068 for the wt protein
241 could be a negative effect of increased pT654, but the similar result with the T654A
242 mutant suggests that PMA has indirect effects independent of pT654.
243
244 **Single-molecule imaging of the clustering and movement of EGFR**
245 We expressed EGFR (wt and T654A) fused with GFP in CHO-K1 cells and, by using
246 single-molecule imaging, detected cluster size distributions and lateral diffusion
247 movements of EGFR molecules in the plasma membrane (Fig. 10a). Clustering of EGFR
248 was measured as the fluorescence intensity distribution of EGFR spots, and the lateral
249 diffusion movements were measured as the increase in the mean square displacement
250 (MSD) of the spots with time. Both measurements were performed before and after 10
251 min of EGF application to the medium. Application of EGF to the medium induced
252 clustering and immobilization of wt EGFR as we have reported previously(14, 26). The
253 distributions of EGFR cluster size suggest formation of oligomers containing up to more
254 than 10 molecules (Fig. 10b). The convex shapes of MSD curve with time indicate
255 subdiffusion of EGFR molecules (Fig. 10c).
256 Even in the absence of EGF, PMA treatment of cells increased fractions of
257 higher-order wt EGFR oligomers (Fig. 10b left), though diffusion movements were hardly
258 affected by PMA (Fig. 10c left). This oligomerization was not as strong as that induced
259 by EGF in the absence of PMA and application of EGF to the PMA treated cells was not
260 induced further oligomerization at least up to 10 min. For T654A mutant, PMA treatment
261 hardly affected both oligomerization (Fig. 10b right) and movements (Fig. 10c right) in

262 the absence of EGF. These effects of PMA to induce EGFR oligomerization dependent
263 on Thr654 is consistent to pT654-induced oligomerization of TM-JM peptides in
264 nanodiscs. Changes in the cluster size and lateral mobility are summarized in Figure 10d.
265 Application of EGF immediately (< 1 min) induced strong oligomerization and
266 immobilized wt EGFR in cells without PMA treatment. In cells with PMA treatment, EGF
267 did not induce further oligomerization but significantly decreased mobility of wt EGFR
268 until 10 min. EGF also induced immediate strong oligomerization of T654A mutant
269 independent of PMA treatment. T654A mutant was immediately oligomerized after EGF
270 application in cells after PMA treatment, but immobilization took time.
271 In summary, single-molecule measurements suggest three states of EGFR
272 oligomerization depends on pT654 and EGF association (Fig. 10d). PMA treatment of wt
273 EGFR but not T654A mutant induced a medial level of oligomerization, which could be
274 stabilized by pT654. Strong oligomerization observed under the weak pT654 level in wt
275 EGFR and no pT654 in T654A mutant was caused by a distinct mechanism of pT654. On
276 the other hand, it is possible that immobilization of EGFR relates with its tyrosine
277 phosphorylation levels. Immobilization was more evident in T654A mutant in which
278 pY1068 level was higher than that in wt EGFR, and PMA treatment decelerate
279 immobilization and decreased pY1068 both in wt and T654A.
280
281 **Interaction of EGFR with GRB2**
282 We finally measured the interaction of EGFR with GRB2 in living cells using a split
283 luciferase (NanoBiT) assay, in which the C-terminus of EGFR and the N-terminus of
284 GRB2 were conjugated with the large BiT (LgBiT) and the small BiT (SmBiT) of
285 NanoLuc luciferase (27), respectively. The association of EGFR and GRB2 promoted the
286 formation of active luciferase to produce chemiluminescence emission (Fig. 11a). From
287 the timecourses of the NanoBiT signal increases after EGF treatment of cells expressing
288 the wt or T654A mutant EGFR (Fig. 11b), the maximum intensities indicated a dose
289 dependent response to the EGF concentration in the medium (Fig. 11b, c). The maximum
290 intensity was significantly increased after pretreatment with PMA in cells expressing wt
291 EGFR (Fig. 11d), despite the fact that the pY1068 level was reduced after the PMA
292 treatment (Fig. 9c). This effect of PMA was not observed to any extent with the T654A
293 mutant, and the GRB2 association was not increased by this mutation in the absence of
294 PMA, even though the pY1068 level after EGF stimulation was significantly increased
295 in the mutant (Fig. 9c). The increase in GRB2 association observed for wt EGFR after
296 PMA treatment was not likely to be an indirect effect of PMA because it was not observed
297 for the T654A mutant, in which the pY1068 level was also affected by PMA. These results

298 suggest that pT654 promotes the formation of a GRB2 recognition state for EGFR, and
299 that the inhibition of Thr654 phosphorylation prevents a GRB2-EGFR association in spite
300 of enhanced Tyr1068 phosphorylation.
301

302 **Discussion**

303 We have here studied the dimerization and oligomerization of EGFR molecules by
304 reconstituting its TM-JM peptides into nanodiscs. As expected from the positively
305 charged JM-A sequence and accumulation of EGFR in the raft membrane, PS and
306 cholesterol affect the molecular assembly of the TM-JM peptides. Interestingly, these two
307 lipid species each function in a specific fashion i.e. the E_{FRET} distributions between the
308 two TM-JM peptides in the nanodiscs suggested that PS facilitates JM dimerization, while
309 cholesterol induces closer positioning of both the TM and JM domains (Figs. 3 and 4). In
310 addition, cholesterol promoted the oligomeric assembly of TM-JM peptides (Figs. 6 and
311 7). We herein propose schematic models for the formation of the EGFR TM-JM dimers
312 and trimers under various conditions of lipid exposure and Thr654 phosphorylation (Fig.
313 8), in which PS and cholesterol exert competitive effects on dimerization and
314 oligomerization, and pT654 disrupts the PS-induced JM dimer, thus promoting
315 oligomerization of the peptides.

316 It should be noted that the E_{FRET} distribution was broad in every one of our
317 observations in this present study, especially between JM domains, indicating multiple
318 configurations coexisting under each condition. Non-phosphorylated peptide dimers
319 showed a peak at around $E_{FRET} > 0.90$ and > 0.81 both for N- and C-terminus labeling,
320 respectively. We can attribute this configuration to that suggested in a previous NMR
321 study, in which two JM domains form an anti-parallel helix dimer (9). PS stabilized this
322 configuration probably at the JM side of the non-phosphorylated peptide. Acidic lipids
323 are known to interact with the positively charged JM-A domain (18, 28) whereas
324 cholesterol induced more proximation of the two peptides at the both N- and C-termini in
325 the major configuration (E_{FRET} 0.95 and 0.93), which must be distinct from the
326 arrangement containing antiparallel JM helices (Fig. 8). If the TM-JM domains of whole
327 EGFR dimer adopt similar configurations as suggested for the TM-JM peptides in the
328 nanodiscs, the arrangement of two kinase domains indicates namely, the kinase activity
329 would be affected by the lipid composition and by pT654 (Fig. 11e).

330 Cholesterol was found in our current analysis to increase the population of
331 nanodiscs containing three TM-JM peptides with pT654 (Fig. 5). The fluorescence
332 intensity distributions of the two Cy3 probes among the three peptides in the presence of
333 cholesterol suggested that a close trimer was the major configuration (Figs. 6 and 7). The
334 cholesterol-induced oligomerization of TM peptides with a short JM region (to T654) of
335 EGFR in liposomes has been reported previously from NMR analysis (29). In that report
336 however, pT654 in the peptide showed no obvious effect on the oligomerization in PC
337 and PC/cholesterol liposomes (without any acidic lipids), consistent with our current and

338 previous results indicating interplay of acidic lipids and pT654. The induction of
339 oligomerization seems to be a general effect of cholesterol upon α-helix peptides in lipid
340 bilayers (30). While in the PC/PS membrane without cholesterol (Figs. 6 and 7), the
341 probability to adopt a one dimer + one monomer configuration seems to be increased for
342 the non-phosphorylated peptides, likely because peptides have difficulty forming trimers
343 when containing the anti-parallel helix JM dimer, the pT654 event appears to dissociate
344 the JM dimer to help in the formation of the close trimer especially in the presence of
345 cholesterol. If this assumption is correct, oligomer formation will be inhibitory for EGFR
346 kinase activity. Our observed increases in the pY1068 level in the T654A mutant of EGFR
347 (Fig. 9) support this possibility.

348 The antiparallel helix dimer of JM is thought to facilitate asymmetric interaction
349 between the kinase domains of EGFR, and hence its activation, in order to phosphorylate
350 tyrosine residues in the C-tail (11, 31). This tyrosine phosphorylation results in the
351 recruitment of PKC and other threonine kinases from the cytoplasm to the EGFR
352 molecules for the phosphorylation of Thr654, which is known to negatively regulate
353 EGFR signaling (25, 32). Our previous results suggested that the mechanism underlying
354 this negative effect of pT654 is the dissociation of JM dimers in the presence of acidic
355 lipids (19). At the same time, pT654 might induce the oligomerization of EGFR in the
356 presence of cholesterol. Supporting this possibility, our current single-molecule imaging
357 in living cells revealed the oligomerization of unliganded wt EGFR after PMA treatment,
358 which induced pT654 (Fig. 10). We previously reported that oligomers of EGFR formed
359 after cell stimulation with EGF function as the major signal transduction sites for GRB2
360 (14). In addition, our current analyses found an increase in the wt EGFR/GRB2
361 association following PMA treatment (Fig. 11). We speculate that the formation of signal
362 transduction oligomers is enhanced in the medium immobilized and oligomerized state
363 of EGFR molecules (Fig. 10d). Further immobilization and oligomerization were found
364 in our current experiments to be induced by EGF in the absence of PMA for wt EGFR
365 and with or without PMA for the T654A mutant. This process might include EGFR
366 molecules accumulated into the clathrin coated pits (33) and be independent of pT654.
367 Distinct from wt EGFR, the T654A mutation in EGFR suppressed the GRB2 association
368 after EGF association in spite of the higher levels of Tyr phosphorylation at the binding
369 site compared to wt. Thus, even though pT654 is inhibitory for EGFR kinase activity, it
370 promotes signal transduction to the cytoplasmic protein, GRB2.

371 Based on our present results, we propose a model of EGFR signaling regulated
372 by membrane lipids and Thr654 phosphorylation (Fig. 11e). The signal transduction
373 mediated by EGFR is a complex multi-step process. Conformational changes in the

374 extracellular domain of EGFR upon ligand association allow JM domains to form acidic
375 lipid-facilitated anti-parallel JM helix dimers and asymmetric kinase domain dimers. This
376 is the activation process for EGFR kinase. Tyrosine phosphorylation in the kinase-active
377 EGFR dimers recruits PKC from the cytoplasm (34). The association of PLCγ to the
378 EGFR phosphotyrosine for the degradation of PIP_2 is involved in this process. PKC then
379 phosphorylates Thr654 (35), which dissociates anti-parallel JM dimers in the presence of
380 remaining acidic lipids and supports the oligomerization of EGFR in the presence of
381 cholesterol, especially after the removal of acidic lipids around the EGFR molecules. The
382 cholesterol-induced oligomer of EGFR is a major site of interaction with cytoplasmic
383 proteins including GRB2. Thus, a major function of EGFR is shifted from a kinase for
384 self-activation to a scaffold for signal transduction. Thr654 phosphorylation is a key step
385 underlying this role change of EGFR and is not merely an inactivating mechanism. The
386 degradation of PIP_2, a major anionic lipid in the inner leaflet of the plasma membrane,
387 may support this role change. Importantly, both Thr654 phosphorylation and PIP_2
388 degradation are caused by the kinase activation of EGFR. Hence, this represents an
389 ingenious autoregulatory process involving membrane proteins and lipids.
390

Materials and Methods

Materials

1-palmitoyl-2-oleoyl-*sn*-phosphatidylcholine (PC), 1-palmitoyl-2-oleoyl-*sn*-phosphatidylserine (PS), and cholesterol were purchased from Avanti Polar Lipids (Alabaster, AL) as chloroform solutions (PC and PS) or powders (cholesterol). Cy3-maleimide and Cy5-maleimide were purchased from GE Healthcare Life Sciences (Little Chalfont, UK). n-octyl-b-D-glucoside (OG) was purchased from Dojindo (Kumamoto, Japan). Monofunctional polyethylene glycol-succinimidyl valerate (s-PEG, 5000 mol wt) and biotinylated monofunctional polyethylene glycol-succinimidyl valerate (b-PEG, 5000 mol wt) were purchased from Laysan Bio (Arab, AL). Chinese hamster ovary K1 (CHO-K1) cells were provided from RIKEN BRC through the National Bio-Resource Project (MEXT, Tokyo, Japan).

Plasmid construction

Construction of the cDNA of full-length human EGFR (wt) fused with GFP was described previously (14). T654A mutant DNA was constructed using PrimeSTAR Max (Takara, Kusatsu, Japan) in the wt EGFR vector. The primer sequences were as follows: EGFR(T654A)-f: GAAGCGCGCGCTGCGGAGGCTGCTGC and EGFR(T654A)-r: CCGCAGCGCGCGCTTCCGAACGATGTG, respectively. For NanoBiT assays, full-length human EGFR (wt or T654A mutant) was fused with LgBiT at the C-terminus (wt or T654A EGFR-LgBiT), and GRB2 was fused with SmBiT at the N-terminus (GRB2-SmBiT) as follows. The LgBiT fragment amplified from pBiT1.1-C [TK/LgBiT] Vector (Promega) using KOD One PCR Master Mix (TOYOBO) was subcloned into the AgeI- and NotI-digested EGFP-N1 vector (Clontech), and subsequently full-length EGFR fragment was subcloned into the NheI- and HindIII-digested the LgBiT-inserted EGFP-N1 vector. The GRB2-SmBiT fragment was constructed using KOD One PCR Master Mix (TOYOBO), and subcloned into the AgeI- and SalI-digested EGFP-C2 vector (Clontech). The primer sequence of SmBiT was designed from pBiT2.1-N [TK/SmBiT] Vector (Promega).

Peptide synthesis and purification

Peptides corresponding to the TM-JM regions of EGFR (618-666) were synthesized by solid-phase methods with the sequence KIPSIATGMVGALLLLLVVALGIGLFM-RRRHIVRKRT$_{654}$LRRLLQERELVE-NH$_2$ (28). For the experiments with the C-terminal labeled EGFR peptide, peptides containing a cysteine at the C-terminus were synthesized. These synthetic peptides were purified by reverse-phase high-performance liquid

427 chromatography on a C4 column with a gradient of 1-propanol and acetonitrile (1:1) over
428 0.1% aqueous trifluoroacetic acid. To prepare the C-terminal labeled peptide, Cy3-
429 maleimide or Cy5-maleimide was introduced to the sulfide group on the cysteine at the
430 C-terminus of the TM-JM peptide by mixing the peptide and the fluorescence derivative
431 in dimethyl formamide under basic conditions. For experiments with the N-terminal
432 labeled peptide, Cy3-COOH or Cy5-COOH was reacted with an elongating peptide on
433 the resin in the presence of 1-[bis(dimethylamino)methylene]-1H-benzotriazolium 3-
434 oxide hexafluorophosphate (HBTU) and diisopropylethylamine (DIEA), which activate
435 the carboxyl group on the fluorophore derivative. For synthesis of Thr654 phosphorylated
436 peptides, phosphorylated threonine derivatives were utilized. The purity was confirmed
437 by reverse-phase high-performance liquid chromatography and matrix-assisted laser-
438 desorption/ionization time-of-flight mass spectroscopy analysis.
439
440 **Nanodisc preparation**
441 For nanodisc construction, fluorescent EGFR TM-JM peptides co-solubilized with lipids
442 and OG in hexafluoroisopropanol were first dried to form thin films. These peptide films
443 were then resolubilized in buffer A (0.5 M NaCl, 20 mM Tris/Cl, 0.5 mM EDTA)
444 containing 30 mM OG and 5 mM dithiothreitol (pH 7.5). His8-tagged MSP 1E3D1 (MSP)
445 was expressed in *E.* coli and purified as described previously (36). The concentration of
446 MSP was quantified based on the absorbance at 280 nm (29,910 $M^{-1}cm^{-1}$). Thin PC or PS
447 films were formed by evaporation of the solvent (chloroform) under a steam of nitrogen
448 gas and dried in vacuum. Cholesterol powders were first dissolved in chloroform, and a
449 thin film was formed as described above. PC, PS, and cholesterol were resuspended in
450 buffer A containing 0.4 M sodium cholate (pH 7.5) at a final concentration of 10 mM.
451 Cy3- and Cy5-labeled TM-JM peptides in buffer A were mixed in equal amounts and then
452 conjugated with MSP and phospholipid mixtures (PC, PC/PS, PC/cholesterol,
453 PC/PS/cholesterol) at a molar ratio of 1:1:120 μM (TM-JM/MSP/lipids). The mixture was
454 dialyzed against a buffer containing 0.5 M NaCl, 20 mM Tris/Cl, and 5 mM EDTA (pH
455 7.5) at 4°C to reconstitute the nanodiscs by removing the detergent. The aggregates and
456 liposomes were removed from the mixture by size-exclusion chromatography using a
457 Superdex 200 Increase column (GE Healthcare Life Sciences) and the peak fractions
458 containing nanodiscs of around 11 nm in diameter were collected.
459
460 **Single-pair FRET (spFRET) measurements**
461 Nanodisc samples were immobilized on the surface of a glass chamber as described
462 previously (19, 37, 38). Briefly, amine-modified glass surfaces were coated with 99% s-

PEG and 1% b-PEG. NeutrAvidin (Thermo Fisher Scientific、Waltham, MA) was then bound to the b-PEG. The nanodisc samples bound with biotinylated anti-His8-tag antibody (MBL Life Science) were loaded into the glass chamber and allowed to bind to the NeutrAvidin-coated glass surface, after which unbound nanodiscs were washed away. To reduce the photobleaching rate of Cy3 and Cy5, the nanodisc-loaded chamber was filled with dialysis buffer containing 2-mercaptoethanol at the final concentration of 0.5% (w/v). The fluorescence of Cy3 and Cy5 was observed under a TIRF microscope based on an inverted microscope (Ti2; Nikon) with a 60x oil-immersion objective (ApoTIRF 60x 1.49 NA; Nikon). The fluorescence activity of Cy3 was excited using a 532 nm laser (Compass 315M-100). Dual-color imaging was carried out through a 4x relay lens by using two EMCCD cameras (C9100-134, ImagEM; Hamamatsu Photonics, Hamamatsu, Japan) with a 200x EM gain. Images of 512 x 512 pixels (67 nm/pixel) were recorded with a temporal resolution of 100 ms/frame using MetaMorph (Molecular Devices, San Jose, CA) or AIS (ZIDO, Toyonaka, Japan).

Analysis of FRET signals

The measurement of fluorescence intensities of single nanodiscs was performed using ImageJ software, as described previously (39). The background noise was filtered out using the Subtract Background function in ImageJ. Fluorescence intensities of Cy3 and Cy5 in single nanodiscs were measured as averages from circles with a diameter of 12 pixels containing a fluorescence spot. The average intensity of the same sized circles in which no spot was present was subtracted as the background. Along the fluorescence trajectories of TM-JM-Cy3 and TM-JM-Cy5, the FRET efficiency, E_{FRET}, for each frame (> 2000) was calculated from the fluorescence intensities in the donor I_{D} and FRET I_{A} channels as

$$E_{FRET} = \frac{I_A - \beta I_D}{I_A + (\gamma - \beta) I_D},$$

where β and γ are coefficients for the compensation of fluorescence leakage from the donor dye to the acceptor detector channel, and the difference in the detection efficiencies of the dyes, respectively (40). Coefficients were calculated using the intensity time traces as $\beta = 0.03$ and $\gamma = 0.4$, respectively. All E_{FRET} distributions were not identical in Kolmogorov-Smirnov (KS) test with a rejection $p < 0.006$. KS test was done using "StatsKSTest" in Igor Pro 8.0 (WaveMetrix). The peak positions and their 95% percentile section were estimated using bootstrap method from the discretized E_{FRET} distribution (Table I), in which the bin width was set to 0.02 and the resampling number was 300.

497 Resampling was done using “sample” function in R.
498
499 **Cell culture and transfection**
500 CHO-K1 cells were maintained in HAM F12 medium supplemented with 10% fetal
501 bovine serum at 37°C under 5% CO_2. HEK293S cells were maintained in DMEM F12
502 medium supplemented with 10% fatal bovine serum at 37°C under 5% CO2. For western
503 blotting assays, DNA constructs of full-length wt and T654A EGFR (1 μg) were
504 transiently transfected into CHO-K1 cells using FuGENE HD Transfection Reagent
505 (Promega, Madison, WI). For single-molecule measurements, CHO-K1 cells were
506 transfected with either a wt or T654A EGFR-GFP gene (0.5 μg each) using Lipofectamine
507 3000 Reagent (Thermo Fisher Scientific). For NanoBiT assays, HEK293S cells were
508 transfected with a mixture of wt or T654A EGFR-LgBiT gene (1 μg each) and GBR2-
509 SmBiT (0.2 μg) using Lipofectamine 3000 Reagent in 60 mm dish.
510
511 **PMA treatment and EGF stimulation**
512 DNA constructs of full-length wt and T654A EGFR were transfected and cultured with
513 10% fetal bovine serum (FBS) on the day before each measurement. Cells were then
514 starved in modified Eagle’s medium without FBS for 3 hours before the experiment.
515 Phorbol 12-myristate 13-acetate (PMA) was dissolved in DMSO and subsequently
516 diluted in PBS to a final concentration of 10 μM. For PMA pre-treatment, PMA solution
517 was added to the cell cultured medium at a final concentration of 100 nM and incubated
518 for 30 min at room temperature. For EGF stimulation, EGF (PeproTech, Cranbury, NJ)
519 dissolved in PBS was added to the cell cultured medium at a final concentration of 100
520 ng/mL (for western blotting assays and single-molecule measurements) or as a 0.001 to
521 100 nM dilution series (for the NanoBiT assay).
522
523 **Western blotting analysis**
524 In cells stimulated with EGF for 0, 5, 30 min at 37°C, threonine and tyrosine
525 phosphorylation of the wt and mutant T654A proteins was detected by western blotting
526 using rabbit anti-pT654 (ab75986; Abcam, Cambridge, UK) and rabbit anti-pY1086
527 antibody (#4407; Cell Signaling Technology, Danvers, MA), respectively. Rabbit anti-
528 EGFR antibody (#sc-03; Santa Cruz Biotechnology, Dallas, TX) was used to detect
529 protein expression. After being resolved by SDS-polyacrylamide gel electrophoresis
530 (PAGE), the electrophoresed proteins were transferred onto a polyvinylidene difluoride
531 (PVDF) membrane and incubated with each antibody (primary antibody) and then with a
532 horseradish peroxidase (HRP)-linked anti-rabbit IgG (secondary antibody; 7076, Cell

533 Signaling Technology). Immunoreactive proteins were detected with Amersham ECL
534 Prime Western Blotting Detection Reagent (GE Healthcare) using an ImageQuant LAS
535 500 device (GE Healthcare).
536
537 **Single-molecule imaging in living cells**
538 The methods for single-molecule measurement and analysis were described elsewhere
539 (Yanagawa and Sako, Methods in Mol Biol, in press; bioRxiv: doi:
540 10.1101/2020.06.08.141192). The single-molecule imaging of EGFR was performed at
541 the basal plasma membrane of the CHO-K1 cells at 25°C with the same microscopic
542 methods used for the spFRET measurements. The laser wavelength was 488 nm (Sapphire
543 488; Coherent, Santa Clara, CA) for the excitation of the GFP. Fluorescence images were
544 acquired every 50 ms using AIS software. The acquired multiple TIFF files were
545 processed by ImageJ software as follows: background subtraction was performed with a
546 rolling ball radius of 25 pixels, and two-frame averaging of the images was then
547 performed. Single-molecule tracking analysis was performed with AAS software (ZIDO).
548 All subsequent analyses were performed using smDynamicsAnalyzer
549 (https://github.com/masataka-yanagawa/IgorPro8-smDynamicsAnalyzer), an Igor Pro
550 8.0-based homemade program.
551
552 **NanoBiT assay**
553 HEK293S cells co-transfected with the plasmids of wt or T654A EGFR-LgBiT and
554 GRB2-SmBiT. Overnight after the transfection, cells were collected in 0.5 mM EDTA-
555 containing PBS, centrifuged, and suspended in 2 mL of HBSS containing 0.01 % bovine
556 serum albumin and 5 mM HEPES (pH 7.4) (assay buffer). The cell suspension was
557 dispensed in a 96-well white bottom plate at a volume of 80 μL per well and loaded with
558 20 μL of 25 μM Nano-Glo Vivazine Live Cell Substrates (Promega) diluted in the assay
559 buffer. After incubation for 2 hrs at room temperature, cells were pretreated with PMA or
560 vehicle as described above. Basal luminescence was then measured by using a microplate
561 reader (SpectraMax L, Molecular Devices) with an interval of 60 sec at room temperature.
562 After 10 min, 20 μL of the EGF dilution series in the assay buffer or the assay buffer
563 (vehicle) were applied to each well using a benchtop multi-pipetter (EDR-384SR, BioTec,
564 Tokyo, Japan) under red dim light. Then, luminescence was measured for 30 min with an
565 interval of 60 sec. Each time-course of luminescence counts was normalized with the
566 luminescence counts of the vehicle-added well. Dose-response curves were fitted with a
567 Hill-equation to determine the maximum intensity.
568

Acknowledgments

YS was supported by MEXT Japan with Grants-in-Aid for Scientific Research (19H05647) and by JST CREST (JPMJCR1912). We thank Hiromi Sato for technical assistance.

Author contributions

Conceptualization, R.M., Y.S.; methodology, R.M., T.S., M.Y., Y.S.; investigation, R.M., H. T., T. S., M.Y.; manuscript writing, R.M., T. S., Y.S. with feedback from all other coauthors; funding acquisition, Y.S.; supervision, Y.S.

Conflicts of interest

None.

582 **References**

583 1. M. A. Olayioye, R. M. Neve, H. A. Lane, N. E. Hynes, The ErbB signaling network:
584 receptor heterodimerization in development and cancer. *EMBO J.* **19**, 3159-3167
585 (2000).
586 2. M. K. Nyati, M. A. Morgan, F. Y. Feng, T. S. Lawrence, Integration of EGFR inhibitors
587 with radiochemotherapy. *Nat. Rev. Cancer* **6**, 876-885 (2006).
588 3. E. Kovacs, J. A. Zorn, Y. Huang, T. Barros, J. Kuriyan, A structural perspective on the
589 regulation of the epidermal growth factor receptor. *Annu. Rev. Biochem.* **84**, 739-764
590 (2015).
591 4. N. J. Bessman, M. A. Lemmon, Finding the missing links in EGFR. *Nat. Struct. Mol.*
592 *Biol.* **19**, 1-3 (2012).
593 5. H. Ogiso *et al.*, Crystal structure of the complex of human epidermal growth factor and
594 receptor extracellular domains. *Cell* **110**, 775-787 (2002).
595 6. X. Zhang, J. Gureasko, K. Shen, P. A. Cole, J. Kuriyan, An allosteric mechanism for
596 activation of the kinase domain of epidermal growth factor receptor. *Cell* **125**, 1137-
597 1149 (2006).
598 7. M. J. Wagner, M. M. Stacey, B. A. Liu, T. Pawson, Molecular mechanisms of SH2- and
599 PTB-domain-containing proteins in receptor tyrosine kinase signaling. *Cold Spring*
600 *Harb Perspect Biol* **5**, a008987 (2013).
601 8. K. M. Ferguson *et al.*, EGF activates its receptor by removing interactions that
602 autoinhibit ectodomain dimerization. *Mol. Cell* **11**, 507-517 (2003).
603 9. N. F. Endres *et al.*, Conformational coupling across the plasma membrane in activation
604 of the EGF receptor. *Cell* **152**, 543-556 (2013).
605 10. E. R. Wood *et al.*, A unique structure for epidermal growth factor receptor bound to
606 GW572016 (Lapatinib): relationships among protein conformation, inhibitor off-rate,
607 and receptor activity in tumor cells. *Cancer Res.* **64**, 6652-6659 (2004).
608 11. N. Jura *et al.*, Mechanism for activation of the EGF receptor catalytic domain by the
609 juxtamembrane segment. *Cell* **137**, 1293-1307 (2009).
610 12. S. E. Webb *et al.*, Single-molecule imaging and fluorescence lifetime imaging microscopy
611 show different structures for high- and low-affinity epidermal growth factor receptors in
612 A431 cells. *Biophys. J.* **94**, 803-819 (2008).
613 13. Y. Huang *et al.*, Molecular basis for multimerization in the activation of the epidermal
614 growth factor receptor. *Elife* **5** (2016).
615 14. M. Hiroshima *et al.*, Transient Acceleration of Epidermal Growth Factor Receptor
616 Dynamics Produces Higher-Order Signaling Clusters. *J. Mol. Biol.* **430**, 1386-1401
617 (2018).

618 15. N. Jura, Y. Shan, X. Cao, D. E. Shaw, J. Kuriyan, Structural analysis of the catalytically
619 inactive kinase domain of the human EGF receptor 3. *Proc Natl Acad Sci U S A* **106**,
620 21608-21613 (2009).
621 16. A. Arkhipov *et al.*, Architecture and membrane interactions of the EGF receptor. *Cell*
622 **152**, 557-569 (2013).
623 17. M. Lelimousin, V. Limongelli, M. S. Sansom, Conformational Changes in the Epidermal
624 Growth Factor Receptor: Role of the Transmembrane Domain Investigated by Coarse-
625 Grained MetaDynamics Free Energy Calculations. *J. Am. Chem. Soc.* **138**, 10611-10622
626 (2016).
627 18. C. Matsushita *et al.*, Transmembrane helix orientation influences membrane binding of
628 the intracellular juxtamembrane domain in Neu receptor peptides. *Proc Natl Acad Sci U*
629 *S A* **110**, 1646-1651 (2013).
630 19. R. Maeda, T. Sato, K. Okamoto, M. Yanagawa, Y. Sako, Lipid-Protein Interplay in
631 Dimerization of Juxtamembrane Domains of Epidermal Growth Factor Receptor.
632 *Biophys. J.* **114**, 893-903 (2018).
633 20. K. B. Abd Halim, H. Koldso, M. S. P. Sansom, Interactions of the EGFR juxtamembrane
634 domain with PIP2-containing lipid bilayers: Insights from multiscale molecular dynamics
635 simulations. *Biochim Biophys Acta* **1850**, 1017-1025 (2015).
636 21. Y. Wang *et al.*, Regulation of EGFR nanocluster formation by ionic protein-lipid
637 interaction. *Cell Res.* **24**, 959-976 (2014).
638 22. Y. Liu *et al.*, The involvement of lipid rafts in epidermal growth factor-induced
639 chemotaxis of breast cancer cells. *Mol. Membr. Biol.* **24**, 91-101 (2007).
640 23. T. Furuchi, R. G. Anderson, Cholesterol depletion of caveolae causes hyperactivation of
641 extracellular signal-related kinase (ERK). *J. Biol. Chem.* **273**, 21099-21104 (1998).
642 24. T. Ringerike, F. D. Blystad, F. O. Levy, I. H. Madshus, E. Stang, Cholesterol is
643 important in control of EGF receptor kinase activity but EGF receptors are not
644 concentrated in caveolae. *J. Cell Sci.* **115**, 1331-1340 (2002).
645 25. K. A. Lund *et al.*, Phosphorylation of the Epidermal Growth-Factor Receptor at
646 Threonine 654 Inhibits Ligand-Induced Internalization and down-Regulation. *J. Biol.*
647 *Chem.* **265**, 20517-20523 (1990).
648 26. M. Hiroshima, Y. Saeki, M. Okada-Hatakeyama, Y. Sako, Dynamically varying
649 interactions between heregulin and ErbB proteins detected by single-molecule analysis
650 in living cells. *Proc Natl Acad Sci U S A* **109**, 13984-13989 (2012).
651 27. A. S. Dixon *et al.*, NanoLuc Complementation Reporter Optimized for Accurate
652 Measurement of Protein Interactions in Cells. *ACS Chem Biol* **11**, 400-408 (2016).
653 28. T. Sato, P. Pallavi, U. Golebiewska, S. McLaughlin, S. O. Smith, Structure of the

654 membrane reconstituted transmembrane-juxtamembrane peptide EGFR(622-660) and
655 its interaction with Ca2+/calmodulin. *Biochemistry* **45**, 12704-12714 (2006).
656 29. D. H. Jones, K. R. Barber, C. W. Grant, The EGF receptor transmembrane domain: 2H
657 NMR study of peptide phosphorylation effects in a bilayer environment. *Biochemistry*
658 **37**, 7504-7508 (1998).
659 30. K. Matsuzaki, Why and how are peptide-lipid interactions utilized for self-defense?
660 Magainins and tachyplesins as archetypes. *Biochim Biophys Acta* **1462**, 1-10 (1999).
661 31. M. Red Brewer *et al.*, The juxtamembrane region of the EGF receptor functions as an
662 activation domain. *Mol. Cell* **34**, 641-651 (2009).
663 32. X. Li, Y. Huang, J. Jiang, S. J. Frank, ERK-dependent threonine phosphorylation of EGF
664 receptor modulates receptor downregulation and signaling. *Cell. Signal.* **20**, 2145-2155
665 (2008).
666 33. L. K. Goh, F. Huang, W. Kim, S. Gygi, A. Sorkin, Multiple mechanisms collectively
667 regulate clathrin-mediated endocytosis of the epidermal growth factor receptor. *J. Cell*
668 *Biol.* **189**, 871-883 (2010).
669 34. K. Oda, Y. Matsuoka, A. Funahashi, H. Kitano, A comprehensive pathway map of
670 epidermal growth factor receptor signaling. *Mol. Syst. Biol.* **1**, 2005 0010 (2005).
671 35. S. Aifa *et al.*, Phosphorylation of Thr654 but not Thr669 within the juxtamembrane
672 domain of the EGF receptor inhibits calmodulin binding. *Biochem. Biophys. Res.*
673 *Commun.* **347**, 381-387 (2006).
674 36. K. Kojima, Y. Imamoto, R. Maeda, T. Yamashita, Y. Shichida, Rod visual pigment
675 optimizes active state to achieve efficient G protein activation as compared with cone
676 visual pigments. *J. Biol. Chem.* **289**, 5061-5073 (2014).
677 37. M. Pirchi *et al.*, Single-molecule fluorescence spectroscopy maps the folding landscape
678 of a large protein. *Nat Commun* **2**, 493 (2011).
679 38. R. Lamichhane *et al.*, Single-molecule view of basal activity and activation mechanisms
680 of the G protein-coupled receptor β_2AR. *Proc. Natl. Acad. Sci. U. S. A.* **112**, 14254-
681 14259 (2015).
682 39. R. Maeda *et al.*, Single-molecule observation of the ligand-induced population shift of
683 rhodopsin, a G-protein-coupled receptor. *Biophys. J.* **106**, 915-924 (2014).
684 40. K. Okamoto, Y. Sako, Variational Bayes Analysis of a Photon-Based Hidden Markov
685 Model for Single-Molecule FRET Trajectories. *Biophys. J.* **103**, 1315-1324 (2012).
686

Figures

Figure 1. Construction of nanodiscs containing fluorescent TM-JM peptides of EGFR. (**a**) Amino acid sequence of the EGFR TM and JM-A domains. EX, extracellular domain; TK, tyrosine kinase domain. (**b, c**) Schematic images of nanodiscs containing dimeric TM-JM peptides fluorescently labeled at the N- (b) and C-terminus (c), respectively. (**d**) Lipid compositions used in the preparation of each nanodisc sample. The fractional ratios of PS and cholesterol mimic those in the mammalian plasma membranes. (**e**) Size-exclusion chromatography used for the purification of nanodiscs containing cholesterol (red) or not (black). The charge ratios of PC/PS/cholesterol are described in the upper table. The fraction having a peak absorbance of around 12 elution volumes (mL) was collected and used for the subsequent experiments. (**f**) A negative stain electron micrograph of fraction 12 in **(e)**. Size distribution of the nanodiscs calculated from the images was fitted with a Gaussian function, with a mean diameter of 11 ± 2 nm.

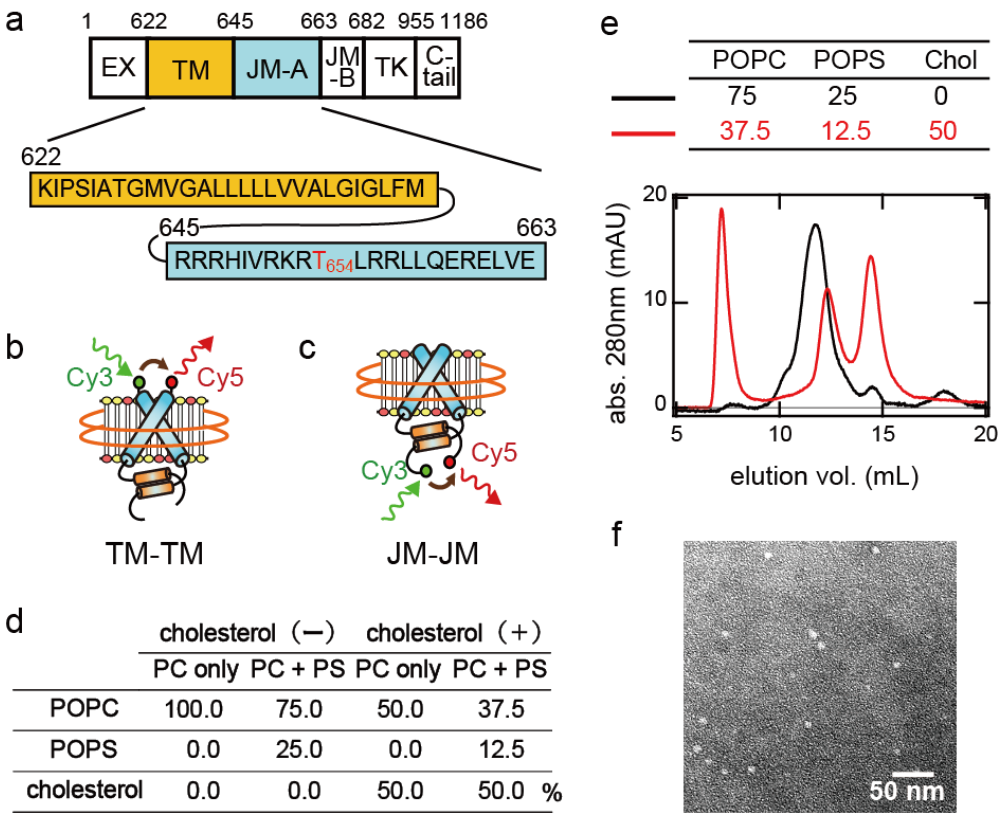

Figure 2. Single-pair FRET measurement of the EGFR TM-JM dimers in nanodiscs. (**a**) Fluorescence micrograph of nanodiscs illuminated with a green laser. Cy3 (green) and Cy5 (red) emissions were superimposed. The Cy5 emission was caused by FRET from Cy3. (**b**) Representative fluorescence trajectories of Cy3 (green) and Cy5 (red). Black allows indicate photobleaching points of Cy5. (**c**) FRET efficiency trajectories of the fluorescence trajectories in **(b)**. The FRET efficiency, E_{FRET}, was calculated as described in the Materials and Methods section. Typical fluorescence and FRET trajectories between peptides labeled at the C-terminus are shown. Transitions to low FRET efficiency states suggested that dissociation of the JM dimer occurred occasionally. The Förster radius R_0 between Cy3 and Cy5 is 5.6 nm.

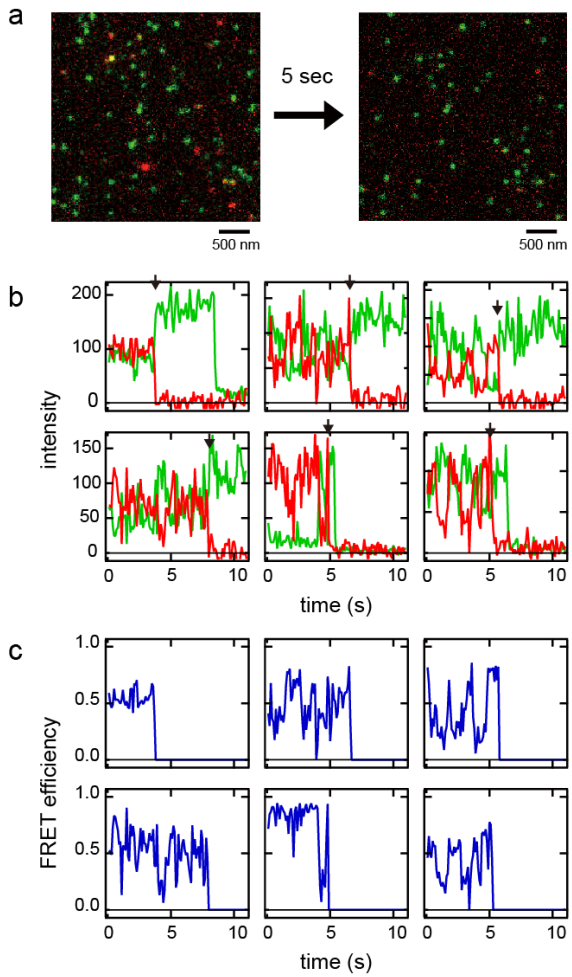

Figure 3. FRET efficiency (E_{FRET}) distributions in nanodiscs containing a single Cy3/Cy5-pair of N-terminal labeled peptides. Nanodiscs contained non-phosphorylated (**a–d**) and Thr654 phosphorylated (**e–h**) peptides at the indicated lipid conditions. In **(b–h)**, the distribution shown in **(a)** (red solid) is superimposed for comparison. The mode and its 95% percentile section are indicated by solid and dashed lines, respectively. Filled area in (b-h) represented the 95% percentile section of (a). See Table I for these values.

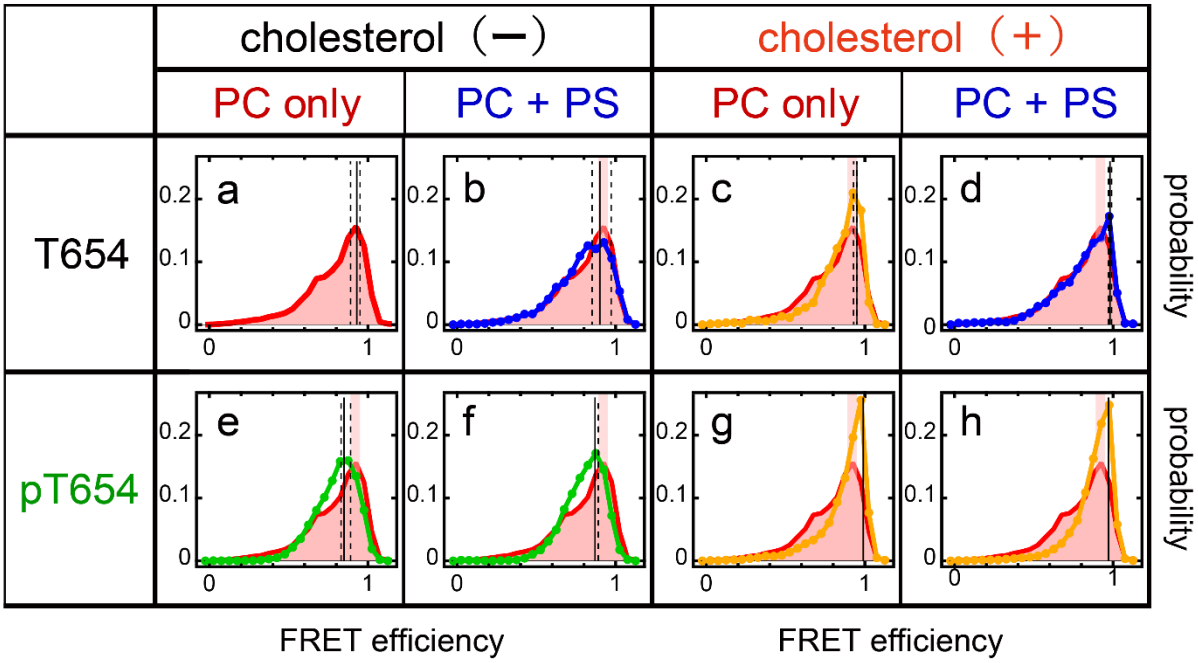

Figure 4. E_{FRET} distributions in nanodiscs containing a single Cy3/Cy5-pair of C-terminal labeled peptides. Nanodiscs contained non-phosphorylated (**a–d**) and Thr654 phosphorylated (**e–h**) peptides in the indicated lipid conditions. In **(b–h)**, the distribution shown in **(a)** (red solid) is superimposed for comparison. The mode and its 5-95% percentile section are indicated by solid and dashed lines, respectively. Filled area in (b-h) represented the 95% percentile section of (a). See Table I for these values.

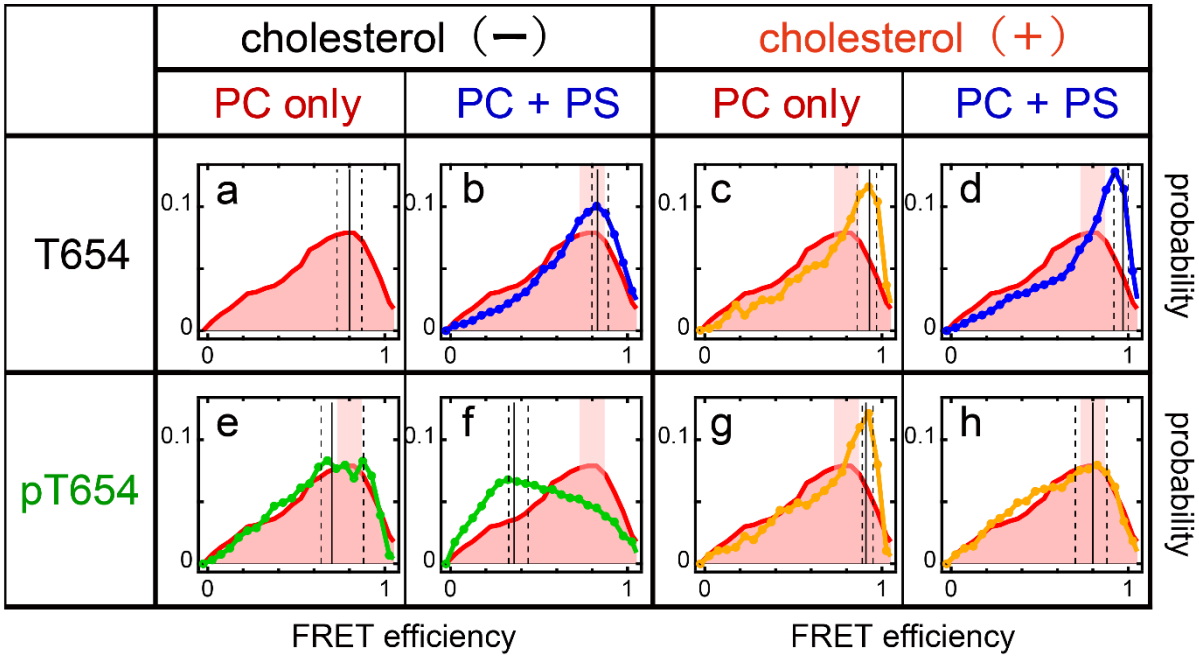

Figure 5. Higher-order oligomerization of EGFR TM-JM peptides in the nanodiscs. Histograms are shown of the total fluorescence intensity of the peptides with Cy3-labeling at the C-terminus in single nanodiscs containing cholesterol (blue) or not (red). Discs containing no Cy5 peptide were chosen for measurement to avoid the possible effects of FRET. Peptides with a non-phosphorylated **(a, c)** or phosphorylated **(b, d)** Thr654 were reconstituted into nanodiscs in PC **(a, b)** or PC/PS **(c, d)** membranes.

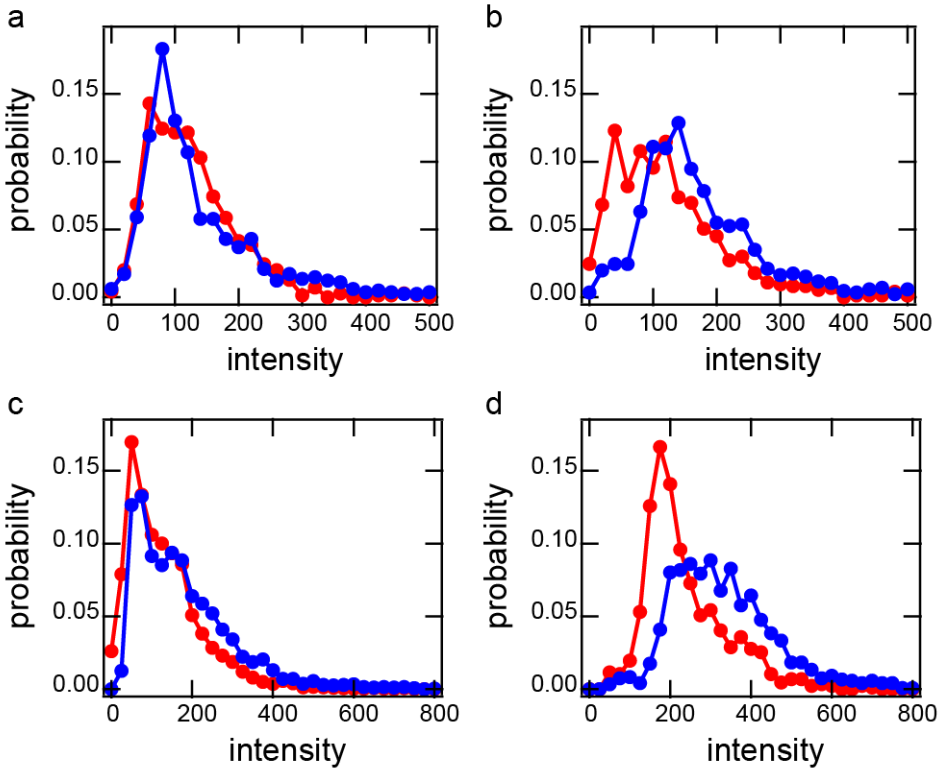

745 **Figure 6**. Assembly of EGFR TM regions. (**a**) Representative fluorescence trajectories of
746 Cy3 (green) and Cy5 (red) in nanodiscs containing two Cy3-labeled and one Cy5-labeled
747 peptide. Fluorescence intensities and/or two-step photobleaching dynamics after Cy5
748 photobleaching indicated that these nanodiscs contained two Cy3 peptides. (**b–i**)
749 Fluorescence intensity histograms of N-terminal-labeled Cy3 peptides before (blue) and
750 after (red) Cy5 photobleaching. Nanodiscs contained non-phosphorylated **(b–e)** and
751 Thr654 phosphorylated **(f–i)** peptides at the indicated lipid conditions. (**j**) Schematic
752 structures indicating proximity between three TM domains before (left) and after (right)
753 Cy5 photobleaching. Note that acceptance of the excitation energy from Cy3 was not
754 saturated for Cy5 under our experimental conditions, even in the presence of two Cy3
755 molecules.
756

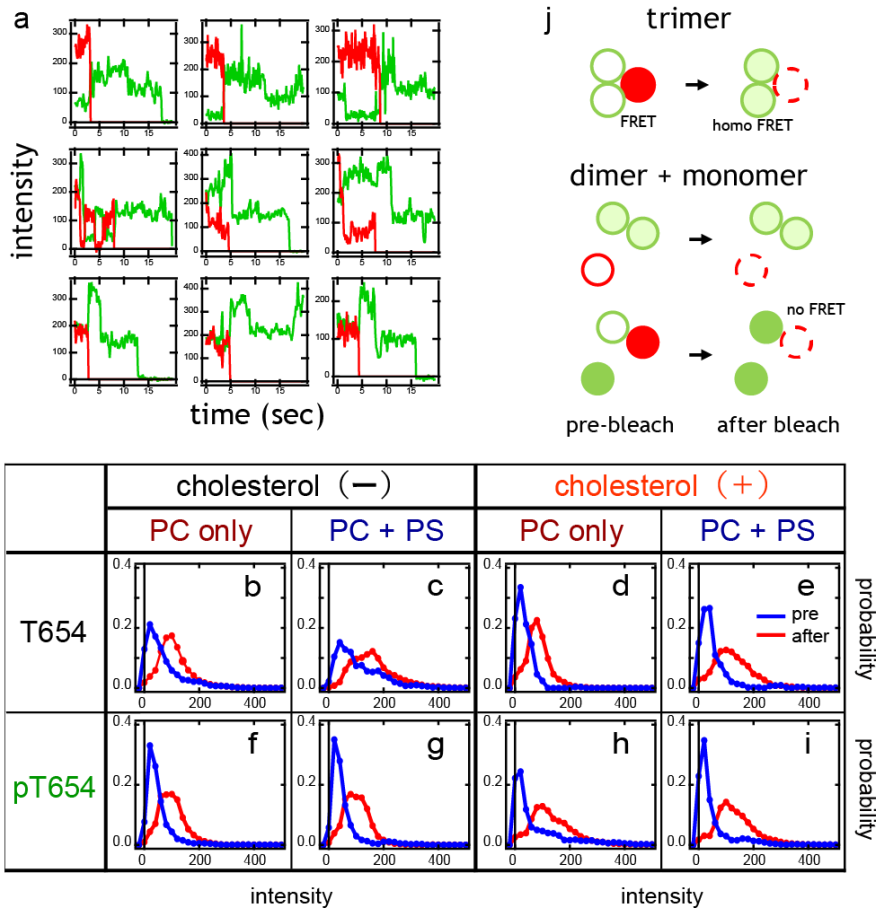

757

Figure 7. Assembly of EGFR JM regions. (**a**) Representative fluorescence trajectories of Cy3 (green) and Cy5 (red) in nanodiscs containing two Cy3-labeled and one Cy5-labeled peptide at the C-terminus. (**b–i**) Fluorescence intensity histograms of C-terminal-labeled Cy3 peptides from nanodiscs containing two Cy3 and one Cy5 peptide before (blue) and after (red) Cy5 photobleaching. Nanodiscs contained non-phosphorylated **(b–e)** and Thr654 phosphorylated **(f–i)** peptides at the indicated lipid conditions. (**j**) Schematic structures indicating proximity between three JM domains before (left and middle) and after (right) Cy5 photobleaching.

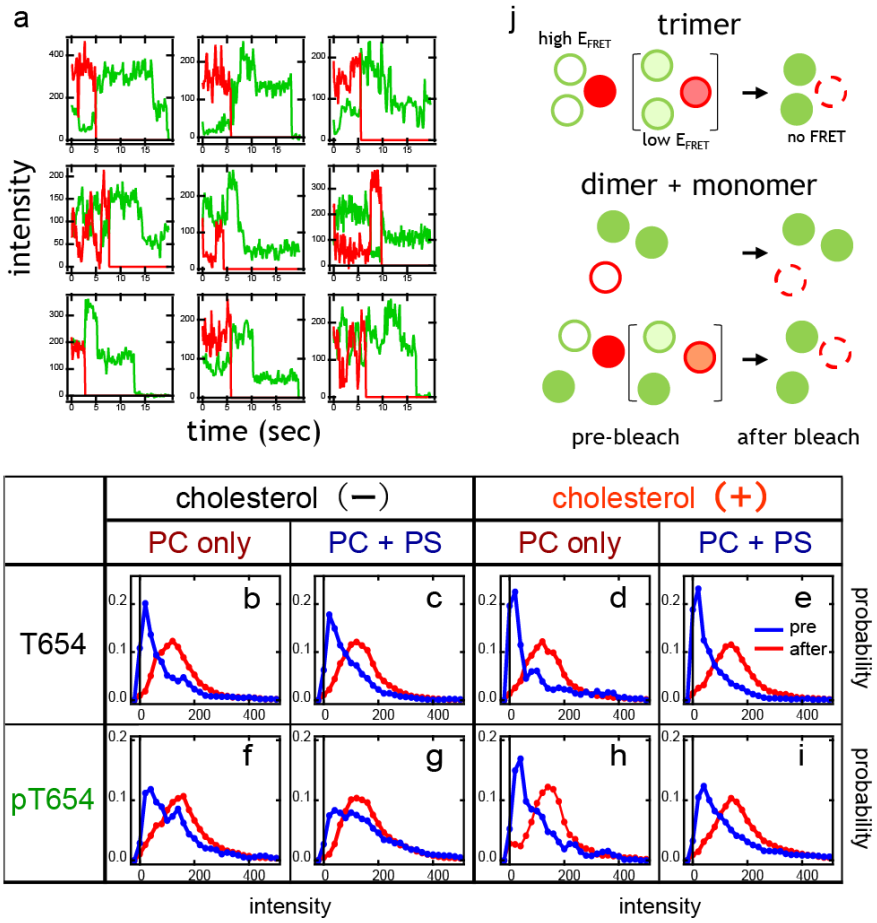

768 **Figure 8.** Possible configurations of EGFR TM-JM dimers and trimers regulated by
769 membrane lipids and Thr654 phosphorylation.
770

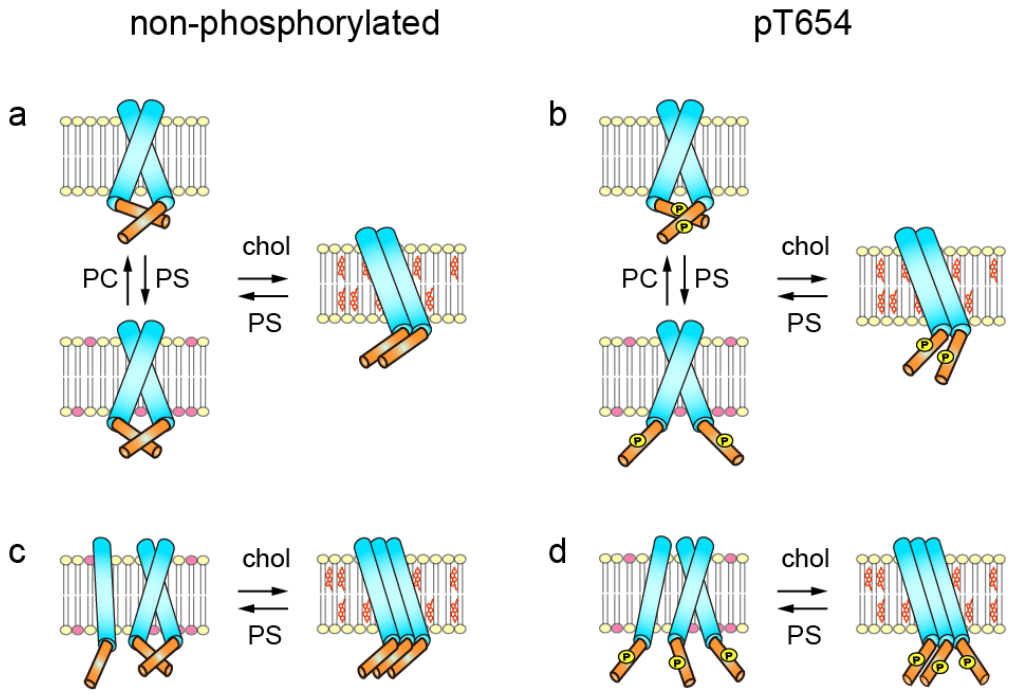

771

Figure 9. Thr and Tyr phosphorylation of EGFR. (**a**) Thr654 phosphorylation after EGF stimulation and PMA treatment. (**b, c**) Timecourses of Y1068 phosphorylation for the wt and T654A mutant of EGFR during EGF stimulation. Typical western blotting results are indicated **(b, top)** and the average of four independent experiments are shown with SE **(c)**. Phosphorylation levels were normalized to the expression levels of the whole EGFR molecule **(b, bottom)**.

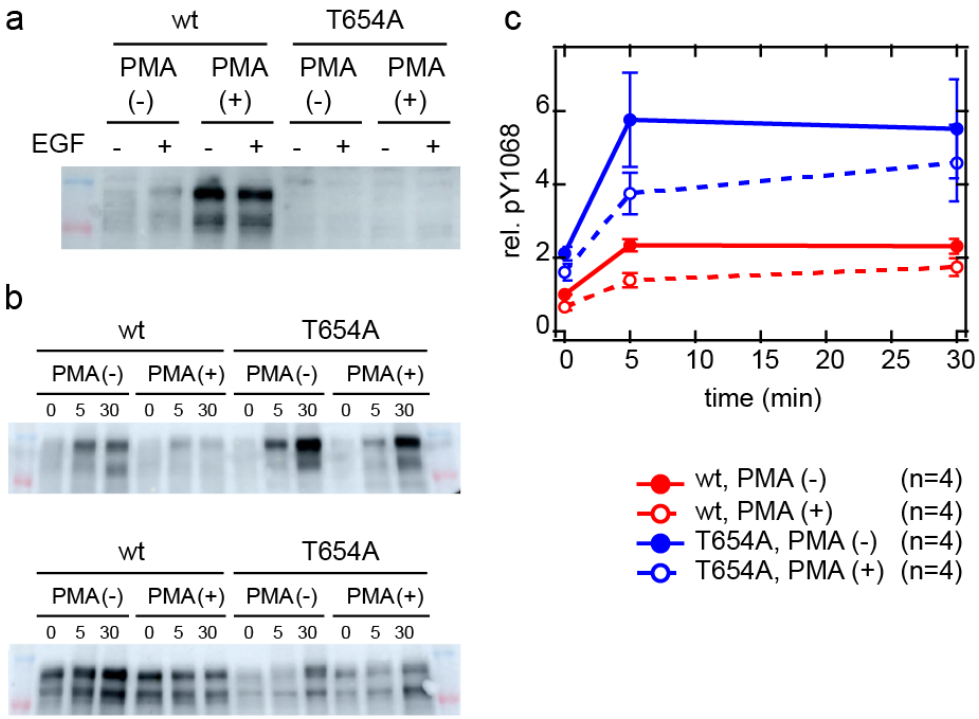

Figure 10. Oligomerization and lateral movements of EGFR on the living cell surface. (**a**) Single molecule imaging of wt EGFR on the surface of living CHO-K1 cells with (right) and without (left) PMA treatment. Cells were stimulated with (lower) and without (upper) EGF. Bar, 5 μm. (**b**) Oligomer size distributions of wt (left) and T654A mutant (right) EGFR in cells. The oligomer size ratio was measured before and 10 min after EGF stimulation. (**c**) Mean square displacement (MSD) of wt (left) and T654A (right) EGFR spots as a function of the time interval, indicating lateral mobility. The MSD was calculated before and 10 min after EGF stimulation. In **(b, c)**, cells were pretreated with (blue, green) or without (black, red) PMA and stimulated (red, green) or not (black, blue) with EGF. (**d**) Diagram of the oligomerization and immobilization states of wt (left) and T654A mutant (right) EGFR suggested from single-molecule measurements. Arrows indicate the state transitions after PMA treatment and EGF stimulation.

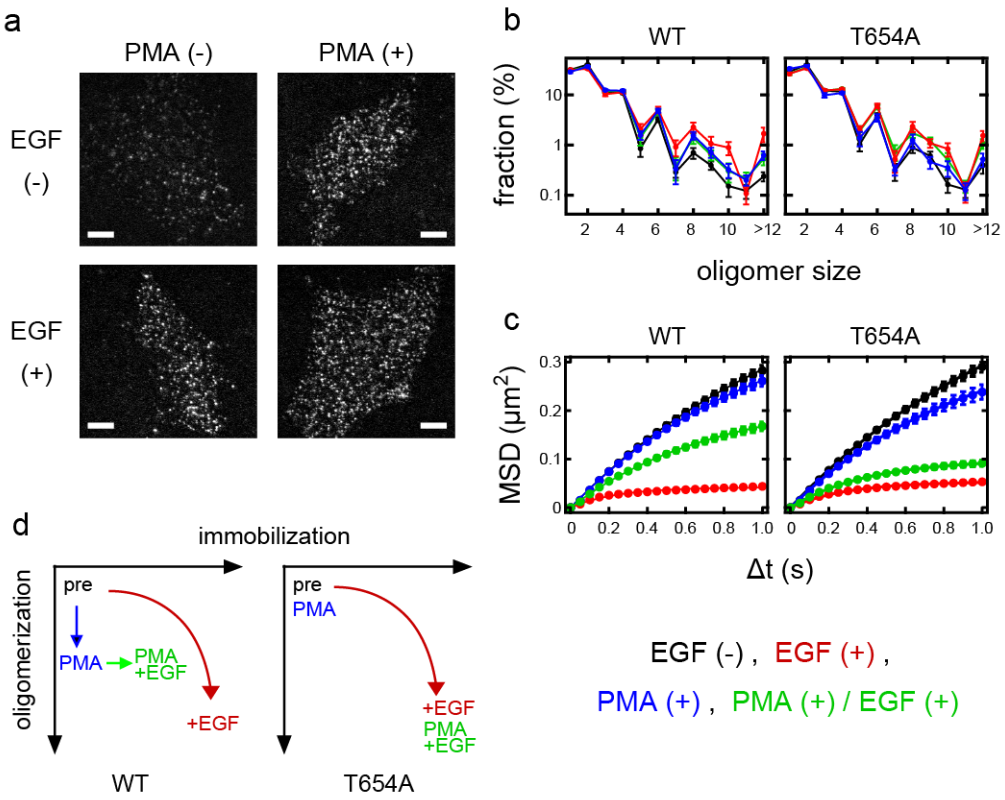

Figure 11. NanoBiT assay for the EGFR/GRB2 interaction in living cells. (**a**) Schematic illustration of the NanoBiT assay of EGFR/GRB2 interactions. (**b**) Typical time courses of chemiluminescence signals generated from the complex formation of large BiT (LgBiT)-fused EGFR and small BiT (SmBiT)-fused GRB2 after EGF application at time 0. The final concentration of EGF in the culture medium was varied from 0.0001 to 100 nM. (**c**) Dose dependency of the chemiluminescence intensities at 30 min after EGF stimulation. The average values from four independent experiments are shown with SE. Lines indicate fitting with a Hill-equation function. (**d**) Maximum intensities of the chemiluminescence signal. The average values from four independent experiments are shown with SE. (*p < 0.05 determined by *t*-test against the signal in wt cells without PMA). (**e**) A schematic model of the activation and signal transduction process for EGFR dimers and oligomers.

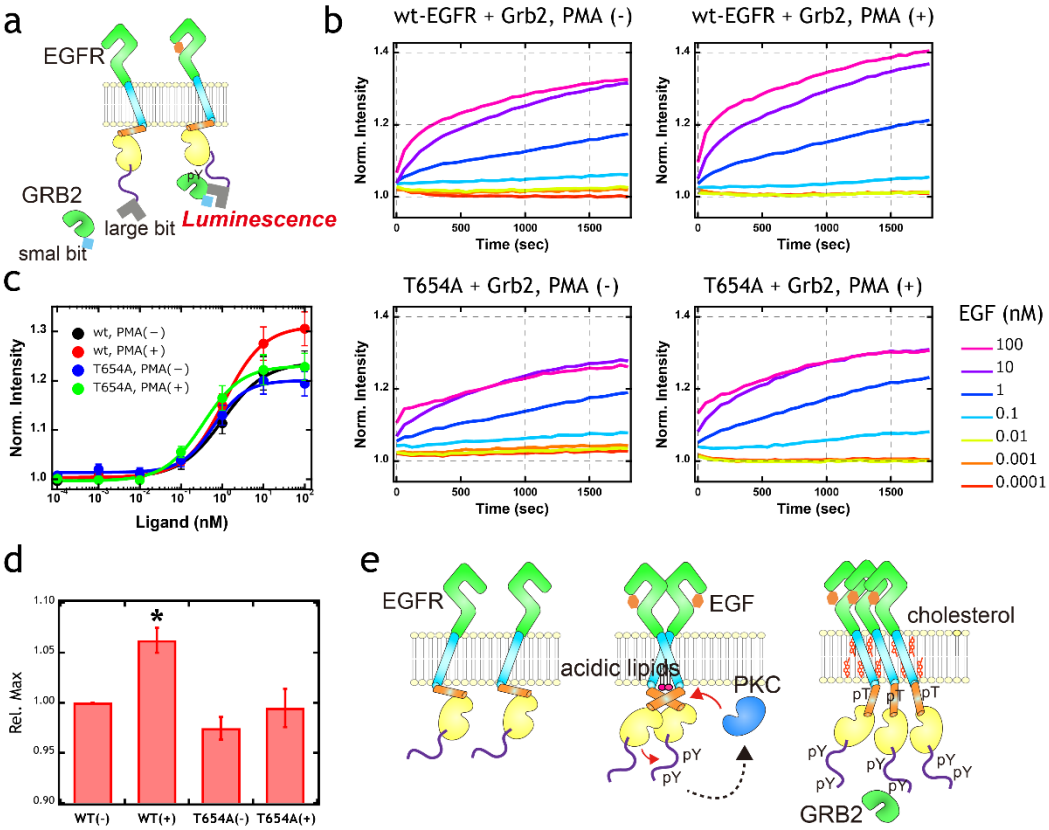

Table I. Peak values in the E_{FRET} distributions between the TM-JM peptides

lipid composition	pT654	labelling			
		N-term		C-term	
		mean	95%	mean	95%
PC	-	0.93	(0.89-0.95)	0.81	(0.73-0.87)
PC/PS	-	0.90	(0.85-0.97)	0.83	(0.79-0.89)
PC/chol	-	0.95	(0.93-0.95)	0.93	(0.85-0.97)
PC/PS/chol	-	0.98	(0.97-0.99)	0.94	(0.91-0.97)
PC	+	0.85	(0.83-0.89)	0.68	(0.63-0.89)
PC/PS	+	0.87	(0.87-0.89)	0.36	(0.33-0.43)
PC/chol	+	0.99	(0.99)	0.90	(0.89-0.95)
PC/PS/chol	+	0.97	(0.97)	0.82	(0.81-0.89)

Mean and their 95% percentile section of the peak values were estimated by bootstrap method with 300-times of resampling. An increase of the resampling times to 1000 did not change the result.